A&A 414, 409–423 (2004)
DOI: 10.1051/0004-6361:20031646

Astronomy & Astrophysics

The physical and chemical structure of hot molecular cores

H. Nomura and T. J. Millar

Department of Physics, UMIST, PO Box 88, Manchester M60 1QD, UK
e-mail: tom.millar@umist.ac.uk

Received 21 July 2003/ Accepted 21 October 2003

Abstract. We have made self-consistent models of the density and temperature profiles of the gas and dust surrounding embedded luminous objects using a detailed radiative transfer model together with observations of the spectral energy distribution of hot molecular cores. Using these profiles we have investigated the hot core chemistry which results when grain mantles are evaporated, taking into account the different binding energies of the mantle molecules, as well a model in which we assume that all molecules are embedded in water ice and have a common binding energy. We find that most of the resulting column densities are consistent with those observed toward the hot core G34.3+0.15 at a time around 10^4 years after central luminous star formation. We have also investigated the dependence of the chemical structure on the density profile which suggests an observational possibility of constraining density profiles from determination of the source sizes of line emission from desorbed molecules.

Key words. molecular processes – radiative transfer – stars: formation – ISM: individual objects: G34.3+0.15

1. Introduction

Hot cores are compact (diameters $\leq$ 0.1 pc), dense ($n \geq 10^7$ cm^{-3}), hot ($T \geq 100$ K), and dark ($A_v \geq 100$ mag) molecular cloud cores. At least some of them are believed to be precursors to ultracompact HII regions and in the early stage of forming massive stars because luminous infrared sources, massive bipolar outflows and/or inflow motion are observed associated with them (e.g., Henning et al. 2000; Kurtz et al. 2000; Churchwell 2002). They are observationally characterized by anomalously large abundances of some molecular species including hydrogenated, saturated, small molecules such as H_2O and H_2S, and large complex molecules such as $HCOOCH_3$ and $(CH_3)_2O$, in contrast to colder dark clouds. It is thought that these molecules are produced under conditions specific to star formation: the freeze-out of gas-phase species onto dust grains and the grain surface reactions in the cold collapsing pre-protostellar phase, and the evaporation of the grain mantle material and the subsequent gas-phase reactions in the hot protostellar phase (e.g., Millar 1993, 1997). Therefore, the observed large column densities of some molecules in hot cores are also expected to be an indicator of luminous high mass star formation which yields a large mass of high temperature gas. Previously, chemical models of hot cores have been studied together with the pre-stellar phase or with some initial conditions of evaporated grain mantle species, and have been successful in reproducing their observational properties (e.g., Brown et al. 1988; Millar et al. 1991; Charnley et al. 1992; Caselli et al. 1993; Charnley 1997; Millar et al. 1997; Viti & Williams 1999; Rodgers & Charnley 2001; Doty et al. 2002).

Physical properties of hot cores have been investigated on the basis of observational studies of molecular line and dust continuum emission. Some physical models together with radiative transfer calculation and/or chemical calculation have succeeded in reproducing the observations of spectral energy distributions and/or molecular column densities (e.g., Millar et al. 1997; Kaufman et al. 1998; Osorio et al. 1999; Hatchell et al. 2000; van der Tak et al. 2000a; Doty et al. 2002). On the other hand, the dynamical processes and the formation mechanisms of massive stars are not yet established because of the difficulty of treating in a self-consistent manner young stellar evolution, the accretion flow and radiation pressure. Non-spherical accretion to protostellar cores, for example, through accretion disks, and/or coalescence of lower mass stars may be involved in massive star formation, but there are, as yet, no accepted theories (e.g., Bonnell et al. 1998; Stahler et al. 2000; Yorke & Sonnhalter 2002). The nature and timescale of the dissipation of the surrounding envelopes of young massive stars, for example, by powerful outflows and ionizing strong winds which stop the accretion, are also uncertain but important in determining the mass of forming stars in the case of the isolated star formation (e.g., Shu et al. 1987; Nakano et al. 1995).

In this paper, we have modeled the density and temperature profiles of hot cores, making use of radiative transfer calculations, and then investigated the hot core chemistry, taking into account the temperature dependent grain mantle

Send offprint requests to: H. Nomura,
e-mail: h.nomura@umist.ac.uk

evaporation. In the following section, we present the physical model of the density profiles constrained by observational results and the temperature profiles calculated by solving the radiative transfer equation. In Sect. 3 we introduce the chemical model along with the temperature dependent grain mantle evaporation process. These models are applied to the hot core G34.3+0.15, and the results of chemical calculation are described and compared with the observations in Sect. 4. Also, we investigate the dependence of the chemical structure of hot cores on (1) the trapping of mantle molecules in water ice and (2) the density profile generally to discuss the chemical and physical condition of massive-star-forming clumps in Sect. 5. Finally, the results are summarized in Sect. 6.

2. Physical model

In this paper we consider a spherically symmetric molecular clump illuminated by a central star with luminosity L_*. The density profiles modeled are constrained by observational results (Sect. 2.1), and the temperature profiles are calculated self-consistently under the assumption of radiative equilibrium by solving the radiative transfer equation (Sect. 2.2).

2.1. Density profiles

As we will see in Sect. 5, the density profile of a clump is one of the crucial properties which affects its chemical structure. However, there is no established theoretical model because the dynamical process of massive star formation is still unknown due to the difficulty in comprehensive treatments of young stellar evolution and accreting flow as well as ionizing radiation, radiation pressure, stellar wind, bipolar outflow, and so forth (e.g., Stahler et al. 2000; Yorke & Sonnhalter 2002). Thus, in this paper we model the density profiles of clumps simply based on the submillimetre observations by Hatchell et al. (2000), avoiding uncertainties in theoretical models.

Hatchell et al. (2000) investigated spectral energy distributions (SEDs) and radial profiles of 450 and 850 μm continuum dust emission of five ultracompact HII regions to conclude that chemically rich hot molecular clumps can be modeled by a combination of compact high density cores plus $r^{-1.5}$ density profile envelopes. Also, van der Tak et al. (2000a) studied 14 envelopes around young massive stars by means of CO, CS, and H_2CO line emission maps, and SEDs and radial profiles of submm dust emission to find that the best-fit values of the power law indices for density profiles of the envelopes range from -1.0 to -1.5. Theoretically, an isothermal self-gravitating gas is known to have r^{-2} density profile via the balance between self-gravity and pressure gradient forces (e.g., Ebert 1955; Bonnor 1956; Larson 1969; Shu 1977). If the non-thermal velocity dispersion, which has been observed in line widths towards various sizes of interstellar clouds and known to have a scaling-law of $\delta v \propto r^{0.5}$ (e.g., Larson 1981; Falgarone et al. 1992; Caselli & Myers 1995), affects the pressure gradient force, it may flatten the radial density profiles of clumps like the logotrope model (e.g., McLaughlin & Pudritz 1996).

Taking into account of these observational and theoretical studies, we use the following spherically symmetric hydrogen number density distribution in this paper:

$$n(r) = \begin{cases} n_0/(1+r/r_c)^2 + n_1/(1+r/r_{tr})^{1.5} & \text{if } r_c < r_{tr}, \\ n_1/(1+r/r_c)^{1.5} & \text{otherwise,} \end{cases} \quad (1)$$

where the radius of $r_{tr} = 0.05$ pc is adopted for the transition between isothermal and nonthermal regions, according to the observations of molecular line widths (e.g., Fuller & Myers 1992; Myers & Fuller 1992). The hydrogen column density of the clumps, $N_H \equiv 2\int_{R_*}^{r_{out}} n(r)dr$, is fixed as $N_H = 10^{25}$ cm^{-2}, based on the observations of the chemically rich hot molecular clumps by Hatchell et al. (2000). The inner radius is set at the stellar surface, R_*, and the outer radius is set at $r_{out} = 1.0$ pc. The central densities n_0 and n_1 are determined to satisfy the relation of $n_0/(1+r_{tr}/r_c)^2 = n_1/(1+r_{tr}/r_{tr})^{1.5}$ and the column density of $N_H = 10^{25}$ cm^{-2}.

2.2. Temperature profiles

The temperature profiles are calculated self-consistently, assuming that the heating source of the clump is a central star with luminosity L_*, under the condition of local radiative equilibrium, that is, the balance between absorption and reemission of radiation by dust grains at each point in the clump:

$$4\pi\int_0^\infty d\nu\kappa_\nu B_\nu[T(r)] = \int_0^\infty d\nu\kappa_\nu \oint d\mu d\phi I_\nu(r;\mu,\phi), \quad (2)$$

where T, κ_ν, and $B_\nu(T)$ represent the temperature, the monochromatic opacity, and the Planck function for blackbody radiation at a frequency ν, respectively. Local thermodynamic equilibrium, $\eta_\nu = \kappa_\nu B_\nu(T)$, is adopted, where η_ν is the monochromatic emissivity. The specific intensity I_ν is calculated by solving the radiative transfer equation,

$$I_\nu(r;\mu,\phi) = \int_0^s \kappa_\nu(r')\rho(r')B_\nu[T(r')]e^{-\tau_\nu(r')}ds', \quad (3)$$

where $\tau_\nu(r')$ is the specific optical depth from r' to r. The short characteristic method in spherical coordinates (Dullemond & Turolla 2000) is used to compute the integration. The radiative transfer equation is solved only in the dusty region (where the dust grains are not thermally destroyed) in this calculation. The inner radius for the numerical calculation is determined as $r_{in} = (T_{in}/T_*)^{-2}R_*$, where T_* and R_* are the temperature and radius of the central star, assuming that the radial profile of the temperature in the dust-free region ($r < r_{in}$) is given by $T(r) \propto r^{-1/2}$, which represents the profile in the optically thin region with gray opacity heated by a point source. For the dust opacity model, we adopt the frequency dependent absorption coefficient κ_ν of Adams & Shu (1985, 1986), which approximates the interstellar dust grains model by Draine & Lee (1984). The dust destruction temperature is set as $T_{in} = 2300$ K in this model (see Nomura 2002 for the details of radiative transfer calculation). In this paper the gas temperature is assumed to be the same as the dust temperature, based on the result of our calculation that the difference between the gas and the dust temperatures is small, except for the very inner region

of the clump, where the gas temperature is $\geq 10^3$ K due to photoelectric heating from small grains induced by the ultraviolet radiation from the central star (cf. Doty & Neufeld 1997).

3. Chemical model

It is generally believed that the relatively large abundances of hydrogenated, saturated, small molecular species, such as H_2O and H_2S, and large complex molecules, such as $HCOOCH_3$ and $(CH_3)_2O$, observed in hot cores are related to the evolution of young stellar objects and the evaporation of grain mantle material. In the cold, pre-stellar phase of the dense molecular clumps the accretion timescale of gas-phase atoms and molecules onto grain surface, $\sim 3\times 10^9/n$ [cm^{-3}] yr at $T = 10$ K, is short enough since the density, n, is high via self-gravitating contraction of the clumps. Thus, the accretion of gas-phase species onto grain surfaces and subsequent surface chemistry produce grain mantles rich in saturated species. Once massive star formation occurs in the clumps, the molecules are evaporated from the grain surface and the subsequent gas-phase reactions produce the large complex molecules seen in the hot gas (see e.g., reviews by Millar 1993, 1997 and references therein), although there is some evidence that even the most complex of molecules may have been formed on grains. On the other hand, the recent detailed analyses of observations of ice absorption features in infrared spectra towards massive young stellar objects have suggested that icy grain mantles in envelopes surrounding the central stars have different composition at different temperatures along the line-of-sight, that is, each icy mantle molecule sublimates from dust grains at a specific temperature (e.g., Ehrenfreund et al. 1998). In this paper, we set the molecular species evaporated from grain mantles as an initial condition, and then calculate the subsequent time-dependent gas-phase chemical reactions, taking into account the different binding energies of the mantle molecules.

The initial fractional abundances of species with respect to total hydrogen nuclei listed in Table 1 are used in this paper. The initial gas is assumed to be mostly molecular and slightly ionized by cosmic rays. The initial mantle composition is determined so as to be consistent with the recent observations of ice absorption features in infrared spectra towards massive young stellar objects (Gerakines et al. 1999; Keane et al. 2001) and other hot core models (Charnley et al. 1992; Millar et al. 1997; Rodgers & Charnley 2001; Doty et al. 2002), and fixed so as to best fit the results of model calculations to observations towards G34.3+0.15 (see Sect. 4). Also, the total abundances of carbon, oxygen, and nitrogen are set to agree with the mean interstellar values of C/H $= 1.4\times 10^{-4}$, O/H $= 3.19\times 10^{-4}$, and N/H $= 7.5\times 10^{-5}$ (Cardelli et al. 1996; Meyer et al. 1997; Meyer et al. 1998).

Each surface species, i, is expected to evaporate thermally with the timescale of

$$\tau_{\mathrm{evap},i} = \nu_{0,i}^{-1} \exp(E_{\mathrm{b},i}/kT), \quad (4)$$

where k and T are the Boltzmann constant and the temperature, respectively. The vibrational frequency $\nu_{0,i}$ is given by $\nu_{0,i} = (2n_{\mathrm{s}}E_{\mathrm{b},i}/\pi^2 m_i)^{1/2}$, where $n_{\mathrm{s}} \approx (7\ \text{Å})^{-1}$ is the number of sites per unit surface area and m_i the mass of the species (e.g., Tielens & Allamandola 1987). The binding energies $E_{\mathrm{b},i}$ are taken from Hasegawa & Herbst (1993), Aikawa et al. (1997), Willacy et al. (1998), and Fraser et al. (2001) (see also references therein). Now, the temperature in the clump is a decreasing function of distance from the central star and assumed to be unchanged with time, while the evaporation rate is very sensitive to the temperature as can be seen from Eq. (4). For example, in the case of water, whose binding energy is $E_{\mathrm{b,H_2O}}/k = 5773$ K, a temperature rise from $T = 95$ K to 105 K shortens the evaporation time by about 1/100. Thus, in this paper the evaporation process is simply modeled:- each species, i, evaporates instantaneously inside a radius $r_{\mathrm{inj},i}$ where the evaporation time $\tau_{\mathrm{evap},i}$ is shorter than the accretion time,

$$\tau_{\mathrm{acc},i} = (S\pi a^2 d_{\mathrm{g}} n v_i)^{-1}, \quad (5)$$

while it is retained on the dust otherwise. That is, the gas-phase abundances of mantle molecules are initially set as those listed in Table 1 inside the injection radii $r_{\mathrm{inj},i}$, and zero outside these radii. Beyond a radius of 1 pc, the density becomes so low that the accretion time becomes comparable to or greater than the chemical time-scales so that mantle formation is not efficient. We do not model this extended envelope here. In Eq. (5) n, a, d_{g}, and $v_i = (2kT/m_i)^{1/2}$ are the number density of hydrogen nuclei, the grain radius, the ratio of the number density of grains to n, and the thermal velocity of the species, i, respectively. The sticking probability S is set as $S = 0.3$. For the grain surface area per hydrogen nucleon, $\pi d_{\mathrm{g}} a^2$, we used the value of $< d_{\mathrm{g}} a^2 > = 2.2\times 10^{-22}$ cm^2 (see Rawlings et al. 1992 for the parameter values). The corresponding injection radii $r_{\mathrm{inj},i}$ in the model of G34.3+0.15 (see next section) are also listed in Table 1. The binding energies of CO and N_2 are low enough and the kinetic temperature high enough that they exist in the gas-phase throughout the region modelled here.

The subsequent gas-phase chemistry is calculated time-dependently by means of the chemical network based on that of Millar et al. (1997), which consists of 209 species connected by 2191 reactions. The standard interstellar cosmic-ray

Table 1. Initial abundances and injection radii of mantle molecules in the model of G34.3+0.15.

Species	Abundance	$r_{\mathrm{inj},i}$[pc]	Species	Abundance	$r_{\mathrm{inj},i}$[pc]
H^+	1.0×10^{-11}		CO	1.3×10^{-4}	
He^+	2.5×10^{-12}		CO_2	3.0×10^{-6}	0.18
H_3^+	1.0×10^{-9}		H_2CO	2.0×10^{-6}	0.3
Fe^+	2.4×10^{-8}		CH_3OH	2.0×10^{-7}	0.12
He	0.1		C_2H_5OH	5.0×10^{-9}	0.14
S	5.0×10^{-9}		O_2	1.0×10^{-6}	0.5
Si	3.6×10^{-8}		H_2O	2.8×10^{-4}	0.08
C_2H_2	5.0×10^{-7}	0.22	N_2	3.7×10^{-5}	
CH_4	2.0×10^{-7}	0.7	NH_3	6.0×10^{-7}	0.17
C_2H_4	5.0×10^{-9}	0.21	H_2S	1.0×10^{-7}	0.29
C_2H_6	5.0×10^{-9}	0.20	OCS	5.0×10^{-8}	0.17

ionization rate, $\zeta = 1.3 \times 10^{-17}$ s^{-1}, is adopted. The adsorption process of neutral atoms and molecules i onto grain surface is included only if $\tau_{\rm acc,}i < \tau_{\rm evap,}i$ in this calculation. The accretion rate is given by

$$k_{{\rm acc},i} = -S\pi a^2 d_{\rm g} n v_i n_i, \quad (6)$$

where n_i is the number density of species i. This process affects the gas-phase abundances slightly in the outer region, but is not very significant because the accretion rate of each species is comparable to the chemical reaction rates.

4. Model of hot core G34.3+0.15

In this section, we model the physical and chemical structure of the hot molecular core G34.3+0.15 using the radiative transfer and the pseudo-time-dependent gas-phase chemistry calculations described in the previous sections together with observations of the spectral energy distribution and the molecular line emissions toward G34.3+0.15. The hot core associated with this source consists of a small clump of hot gas situated at the nose of a cometary-shaped, ultra-compact HII region. It has been well-observed, particularly through spectral line surveys (Macdonald et al. 1996; Kim et al. 2000) at 1, 2 and 3 mm, and has a rich molecular line spectrum, with large abundances of complex, highly-saturated molecules.

4.1. Density and temperature profiles

The density and temperature profiles of the hot core G34.3+0.15 are modeled so that the theoretical calculation of the spectral energy distribution (SED) is consistent with that observed. We take $r_{\rm c}$ defined in Sect. 2.1 as a parameter and obtain its best-fit value by iteratively calculating the temperature profile (see Sect. 2.2) and comparing the resulting SED with observation. The luminosity of the central star is set as $L_* = 4.7 \times 10^5\ L_\odot$, referring to Watt & Mundy (1999). For the temperature and radius of the star we adopt $T_* = 4.5 \times 10^4$ K and $R_* = 11\ R_\odot$, assuming a massive zero-age main-sequence star (e.g., Thompson 1984; see also references therein). The distance to G34.3+0.15 of 3.7 kpc and the observational data for the SED are taken from Chini et al. (1987). As a result of the calculations, we find that the model with $r_{\rm c} = 0.05$ pc represents the best fit to the observational data at wavelengths from far-infrared to millimeter. The resulting density and temperature profiles, and the calculated SED are shown in Figs. 1a, 1b, and 1c, respectively, with solid lines. The crosses in Fig. 1c are the observational data.

The data at wavelengths from near- to mid-infrared can not be reproduced by this model probably because of the inappropriate assumption of the spherically symmetric density profile. For example, the optical depth of non-spherical cavities due to bipolar outflows would be less than that of the dense envelopes so that if we were to observe the inner region of the clumps through optically thin cavities, namely, there would be more flux in the infrared (cf. Hatchell et al. 2000; van der Tak et al. 2000a). Actually, the model with the column density of $N_{\rm H} = 10^{24}$ cm^{-2} (1/10 of the above envelope model) and the core radius of $r_{\rm c} = 0.05$ pc, which is plotted with a dotted line in Fig. 1c, better represents the observational data in the mid-infrared. Here, the bolometric luminosity ratio contributed from the envelope region with $N_{\rm H} = 10^{25}$ cm^{-2} to the cavity region with $N_{\rm H} = 10^{24}$ cm^{-2} is assumed to be 20:1 in order to

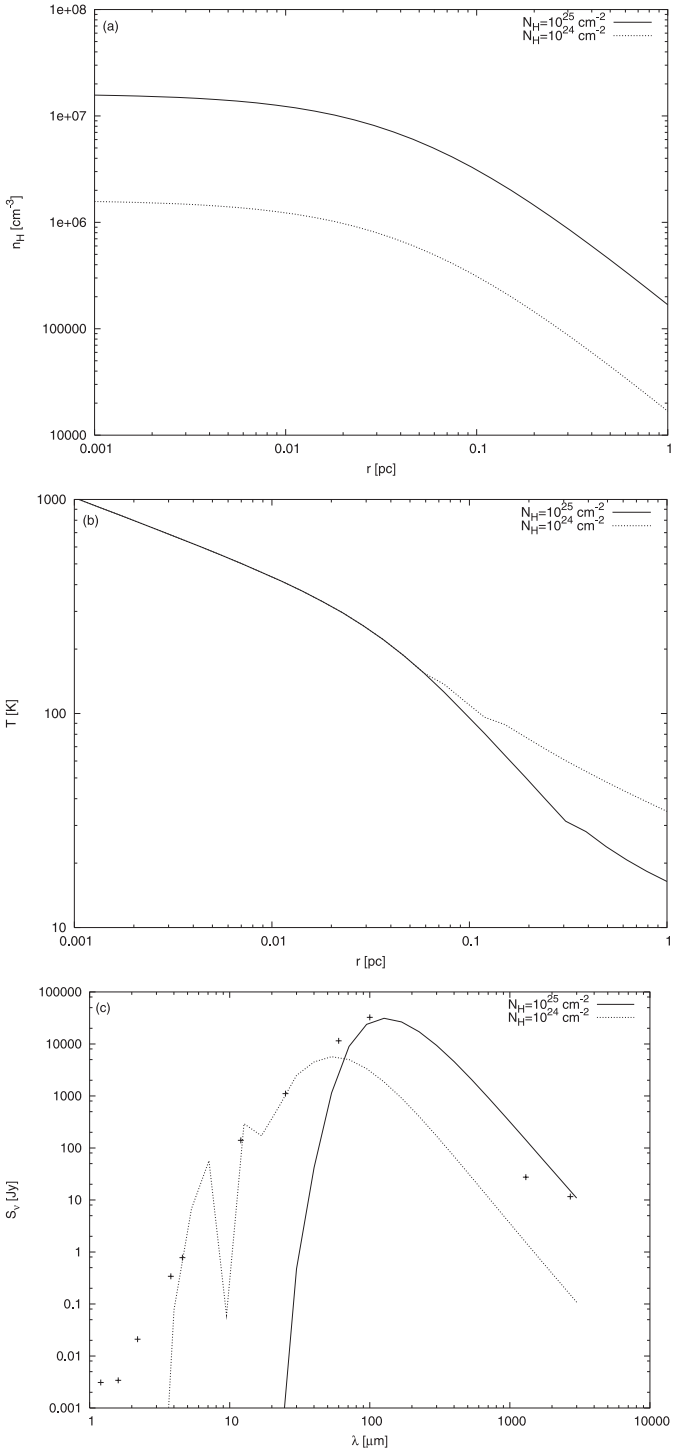

Fig. 1. a) Density and **b)** temperature profiles and **c)** SED of the model of G34.3+0.15. Combination of a envelope with $N_{\rm H} = 10^{25}$ cm^{-2} (solid lines) and a cavity with $N_{\rm H} = 10^{24}$ cm^{-2} (dotted lines), whose core radii are $r_{\rm c} = 0.05$ pc, reproduces the SED observational data (crosses).

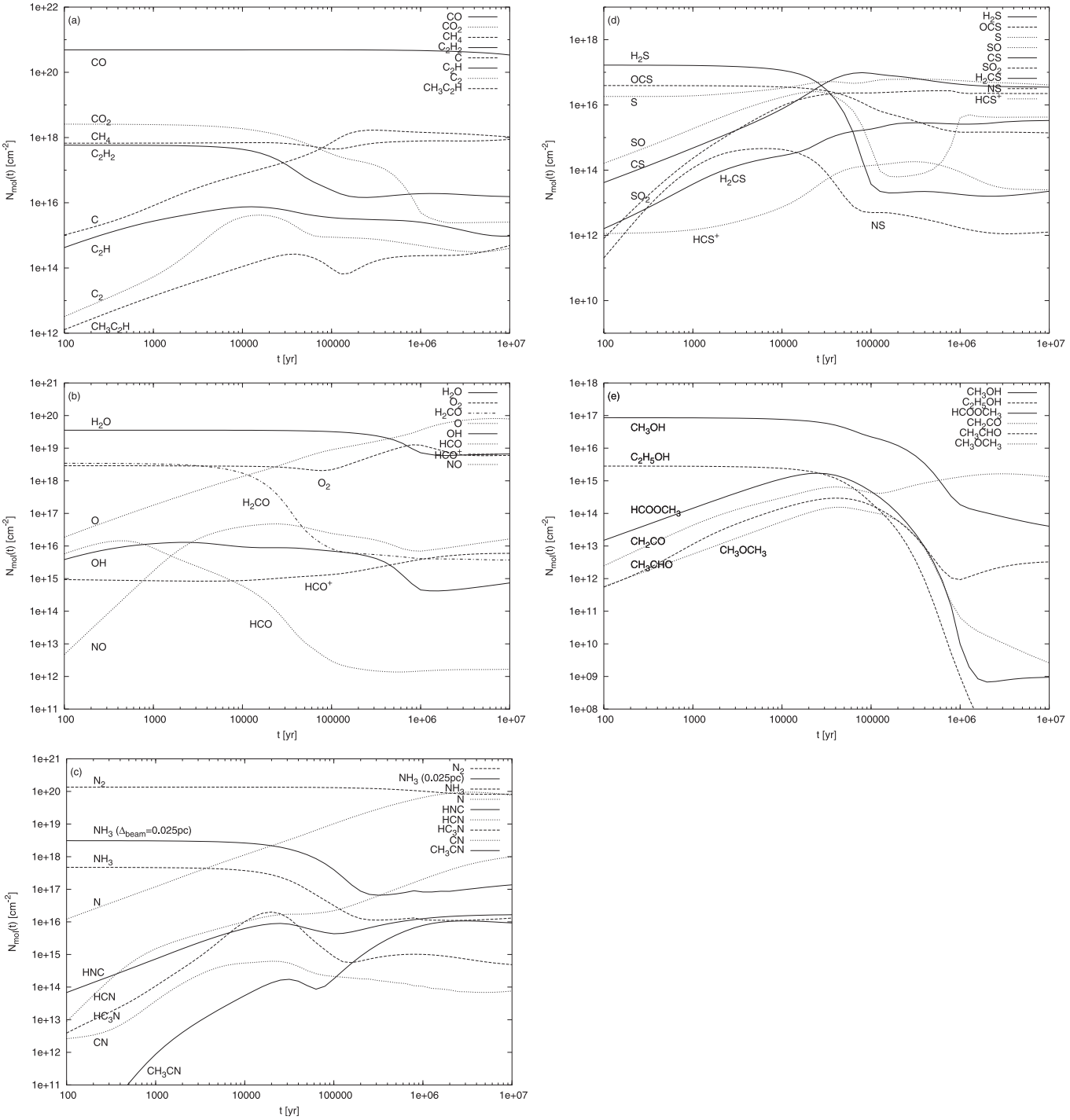

Fig. 2. The time evolution of column densities of some molecules in the model of G34.3+0.15. Parent molecules are eventually destroyed to produce daughter species around the timescale of 10^4 yr.

fit the observational data. This will mean that the solid angle of the cavity will be much less than 4π and/or the radiation flux in the clump around the central star is not spherically symmetric in fact. Its density and temperature profiles are also shown with dotted lines in Figs. 1a,b. In the following subsections, we only use the model with the column density of $N = 10^{25}$ cm^{-2} because most of the mass of the clump will be contained in this dense envelope region rather than the less dense, cavity region.

4.2. Results of chemical calculation

4.2.1. Time evolution of molecular column densities

Making use of the density and temperature structures obtained in the previous subsection and the chemical model in Sect. 3, we simulate the time evolution of the hot core G34.3+0.15. The resulting time evolution of molecular column densities are shown in Fig. 2. In order to compare these with the observations

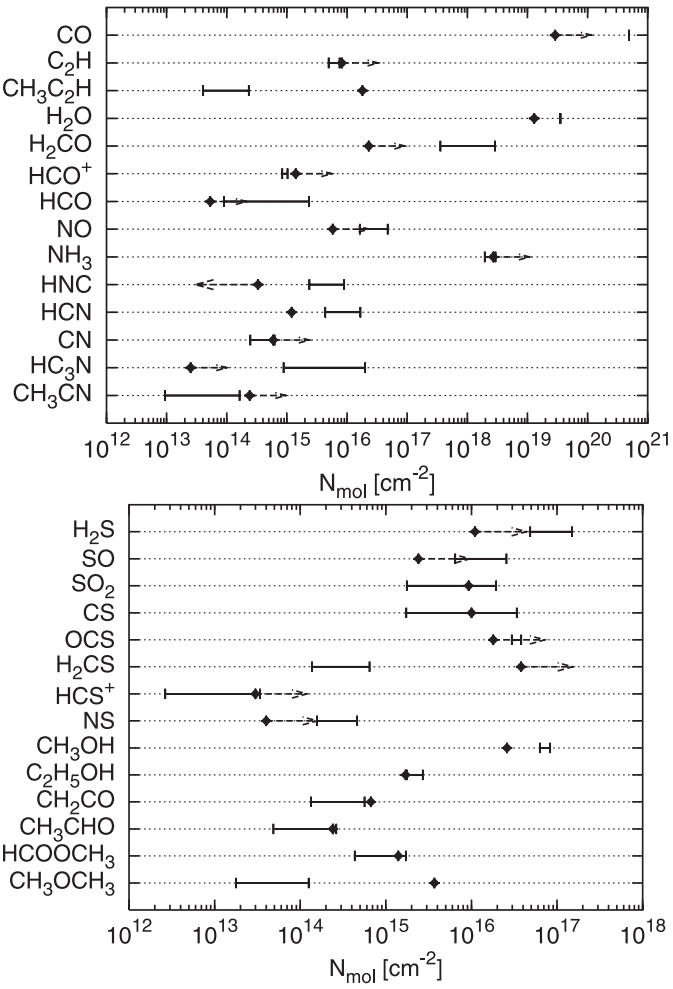

Fig. 3. Comparison between the calculated molecular column densities from 3×10^3 yr to 3×10^4 yr (solid lines) and the observations towards G34.3+0.15 (diamonds plus dotted arrows if they are the lower or upper limits). The results are in good agreement with most of the observations.

of beam-averaged column densities, each atomic or molecular column density is calculated as

$$N_i(t) = \frac{1}{\pi\Theta_{\rm beam}^2} \int_0^\infty 2\pi r \tilde{N}_i(r,t) \exp\left(-\frac{r^2}{\Theta_{\rm beam}^2}\right) {\rm d}r, \quad (7)$$

where $\tilde{N}_i(r,t) = \int_{-\infty}^{\infty} n(s) x_i(s,t) {\rm d}s$ is the column density of species i along a line of sight at a distance r from the clump centre. Here, $n(s)$ is the number density of hydrogen nuclei, $x_i(s,t)$ the fractional abundance of species i at time t, and s the depth along the line of sight. The scale size $\Theta_{\rm beam}$ is simply taken as 0.25 pc which corresponds to the angular size of 13″ at the distance of 3.7 kpc, based on the half power beam width of the James Clerk Maxwell Telescope (JCMT) at 345 GHz (cf. Thompson et al. 1999). While the data of most molecular lines we use in this paper are from single radio telescope observations such as the JCMT, the NH_3 data is from the Very Large Array observation whose synthesized beam size is about 1″3 (Heaton et al. 1989). Thus, we calculate the NH_3 column density with $\Theta_{\rm beam} = 0.025$ pc as well as with $\Theta_{\rm beam} = 0.25$ pc for comparison.

From Fig. 2 we can see that parent molecules, such as H_2O, NH_3, H_2S, and CH_3OH, which are expected to be formed on grain surfaces, are relatively stable for timescales of at least 10^4 yr in this model. However, they are eventually destroyed by ionized species or atomic hydrogen to produce daughter species (see Sect. 4.2.3 for the details) as has been suggested in the previous studies (e.g., review by Millar 1997). Thus, the observed large abundances of both parent and daughter molecules will mean that the ages of the chemically rich hot cores are about 10^4 yr. In particular, we compare the results of our calculation with observations in Fig. 3, which shows that the calculated molecular column densities from 3×10^3 yr to 3×10^4 yr (solid lines) are in good agreement with most of those observed toward the hot core G34.3+0.15 (diamonds plus dotted arrows if they are the lower or upper limits), consistent with the result of Millar et al. (1997). Lower limits in this Table have been derived from optically thick transitions. The calculated molecular column densities, with the exception of CH_3CCH, HNC, H_2CS, and CH_3OCH_3, satisfy the observational lower limits or fit the observations to within a factor 4 at most. Discrepancies may be resolved in a number of ways. Dimethyl ether, CH_3OCH_3, may in fact be a mantle molecule, while the gas-phase chemistry of H_2CS is not at all well understood. Unlike H_2CO, for which efficient gas-phase synthetic pathways have been studied in the laboratory, the analogous reactions which might form thioformaldehyde do not occur. The chemistry of HNC at low temperatures is well understood; the discrepancy between model and observation may imply that additional high-temperature loss mechanisms which are not included in the model are at work. Finally, the methyl acetylene, CH_3CCH, column density is about a factor of 100 less than that observed by Macdonald et al. (1996) from their 330–360 GHz spectral line scan. However, it is much closer to the value of 8.2×10^{14} cm^{-2} determined from the 2 and 3 mm line surveys of Kim et al. (2000), similar to the value derived by Hatchell et al. (1998a) 20″ offset from the hot core. Finally, we note that the formation of $C_3H_5^+$, the precursor ion to CH_3CCH, involves ions and neutrals related to CH_4, C_2H_2 and C_2H_4. An increase in the abundances of each of these parents by a factor of a few would also help resolve the discrepancy noted above. The observational data are taken from Millar et al. (1997) (see also Macdonald et al. 1996; Hatchell et al. 1998a) and Ikeda et al. (2001).

4.2.2. Radial profiles of molecular abundances

In order to see the effects of the temperature dependent injection of molecules from dust grains on hot core chemistry, we present the radial profiles of molecular abundances at 10^4 yr in Fig. 4. We can see from the figures that the abundances of many parent molecules injected from grain mantles, such as C_2H_2, CO_2, H_2O, H_2S, and CH_3OH, change dramatically at $r_{{\rm inj},i}$, inside which the molecule i can be easily evaporated. Inside $r_{{\rm inj},i}$, most of the parents are difficult to destroy. Nevertheless, given their large initial abundances, even a slow

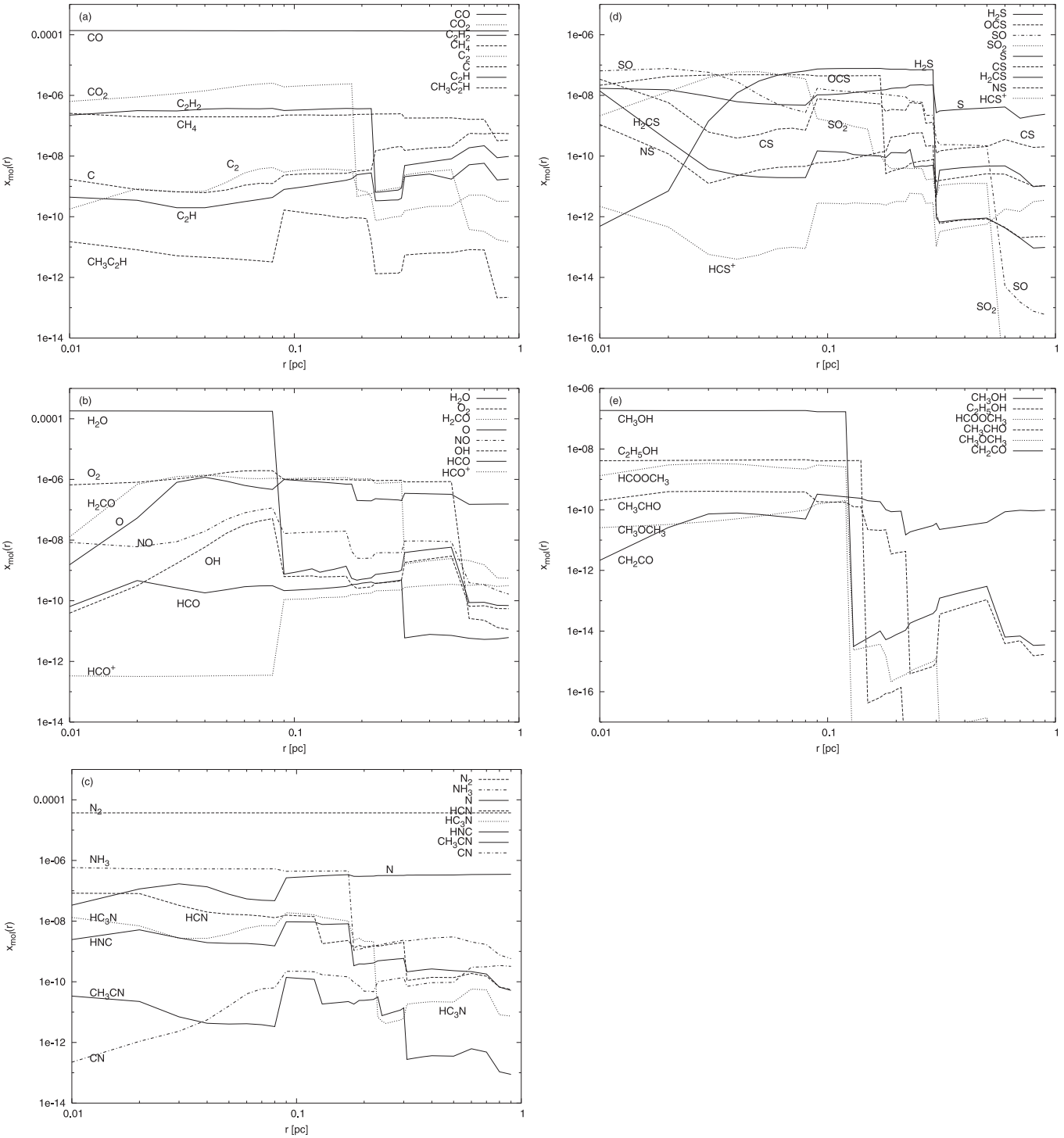

Fig. 4. The radial profiles of some molecular abundances of the model of G34.3+0.15 at 10^4 yr. Some parent, daughter and other related species have dramatic changes at radii related to the grain mantle evaporation.

destruction rate is large enough to produce appreciable abundances of daughter products. Thus, the radial abundance profiles of the parent molecules influence those of daughter and other related species (see Sect. 4.2.3 for details). Abundance changes of some molecules along the radial direction in the clumps around young massive stars have been suggested by observational studies. For instance, the observations of the CH_3CN rotational transition lines indicate that they are emitted from the inner compact hot region of the clumps, while the observed CH_3OH lines suggest that the gas in some clumps consists of at least two components, one of which is hot and abundant in CH_3OH, and the other is cooler and less abundant (Hatchell et al. 1998a; Millar & Hatchell 1998; van der Tak et al. 2000b). In addition, the observational abundances of

the vibration-rotation lines of C_2H_2, HCN, H_2O, and CO_2 are found to increase with the excitation temperature (Lahuis & van Dishoeck 2000; Boonmann et al. 2000). Detailed radiative transfer calculations will be needed to compare the results of our theoretical model with these observations. We note that abundance jumps similar to those predicted have been observed in the low-mass "hot core" around IRAS 16293-2422 (Schöier et al. 2002).

Our results show that a different chemistry operates in the surrounding cooler envelopes from that in the central hot regions where icy mantles can be evaporated, as has been indicated (e.g., Millar et al. 1997; Doty et al. 2002). In order to see the quantitative differences comparable with observations, we calculate the molecular column densities off-centred from the clump centre by a distance $r_{\rm off}$, making use of Eq. (7) with the distance from the clump centre, $r' = r - r_{\rm off}$ replacing r. The results at $t = 10^4$ yr are listed in Table 2. Parameters of $\Theta_{\rm beam} = 0.25$ pc and $r_{\rm off} = 0.4$ pc are adopted for comparing the results with observations toward the halo associated with G34.3+0.15 by Thompson et al. (1999), which are also included in Table 2. For comparison, the molecular column densities calculated around the clump centre by Eq. (7) with $t = 10^4$ yr are also listed together with the observations which are the same as those in Fig. 3. The results of the model calculations are consistent with most of the observations. The ratio of the calculated molecular column densities around the clump centre to those off-centred range roughly from a factor 2, when the radial abundances of the species are almost constant, to one order of magnitude, in the case of parent or daughter species which are hardly generated by the gas-phase reactions without grain mantle evaporation.

Table 2. Molecular column densities: centre vs. off-centre.

	Molecular column density [$\rm cm^{-2}$]			
	Centre		Off-centre	
Species	Model[a]	Observation	Model[a]	Observation
H_2	3.6×10^{24}		2.0×10^{24}	
CO	4.9×10^{20}	$>2.9\times10^{19}$	2.6×10^{20}	$>1.3\times10^{19}$
C_2H	7.4×10^{15}	$>8.2\times10^{15}$	4.9×10^{15}	$>2.9\times10^{14}$
CH_3C_2H	1.1×10^{14}	1.8×10^{16}	1.9×10^{13}	
H_2O	3.5×10^{19}	1.3×10^{19}	4.5×10^{18}	
H_2CO	1.7×10^{18}	$>2.3\times10^{16}$	3.0×10^{17}	$>1.3\times10^{14}$
HCO^+	8.7×10^{14}	$>1.4\times10^{15}$	6.0×10^{14}	$>2.3\times10^{13}$
HCO	6.4×10^{14}	$>5.3\times10^{13}$	1.3×10^{14}	
NO	3.9×10^{16}	$>5.8\times10^{15}$	1.2×10^{16}	
NH_3	3.7×10^{17}		3.9×10^{16}	
NH_3[b]	2.6×10^{18}	$>2.7\times10^{18}$		
HNC	6.2×10^{15}	$<3.3\times10^{14}$	8.6×10^{14}	
HCN	1.0×10^{16}	1.2×10^{15}	1.3×10^{15}	$>2.3\times10^{13}$
CN	5.5×10^{14}	$>5.9\times10^{14}$	3.9×10^{14}	$>9.5\times10^{12}$
HC_3N	1.0×10^{16}	$>2.5\times10^{13}$	9.7×10^{14}	
CH_3CN	5.5×10^{13}	$>2.4\times10^{14}$	6.5×10^{12}	
H_2S	1.2×10^{17}	$>1.1\times10^{16}$	1.9×10^{16}	
SO	1.7×10^{16}	$>2.4\times10^{15}$	2.3×10^{15}	
SO_2	9.3×10^{15}	9.3×10^{15}	9.9×10^{14}	$>2.0\times10^{14}$
CS	7.5×10^{15}	1.0×10^{16}	1.4×10^{15}	$>5.3\times10^{13}$
OCS	3.6×10^{16}	$>1.8\times10^{16}$	3.4×10^{15}	
H_2CS	2.8×10^{14}	$>3.8\times10^{16}$	7.9×10^{13}	
HCS^+	7.3×10^{12}	$>3.0\times10^{13}$	3.6×10^{12}	
NS	4.3×10^{14}	$>4.0\times10^{13}$	8.7×10^{13}	
CH_3OH	7.7×10^{16}	2.6×10^{16}	6.9×10^{15}	$>3.6\times10^{14}$
C_2H_5OH	2.4×10^{15}	1.7×10^{15}	2.3×10^{14}	
CH_2CO	3.0×10^{14}	6.7×10^{14}	1.3×10^{14}	
CH_3CHO	1.4×10^{14}	2.4×10^{14}	1.5×10^{13}	
$HCOOCH_3$	1.1×10^{15}	1.4×10^{15}	9.2×10^{13}	
CH_3OCH_3	5.6×10^{13}	3.7×10^{15}	5.0×10^{12}	

[a] Calculated results at 10^4 yr.
[b] In the case of $\Theta_{\rm beam} = 0.025$ pc.

4.2.3. Detailed chemistry

In this subsection, we discuss some of the hot core chemistry, mainly focusing on the effects of the injection of parent molecules from grain mantles on the radial abundance profiles of daughter and other related species.

Figures 2a, b show the time evolution of column densities of the carbon- and oxygen-bearing species, while Figs. 4a, b represent the radial profiles of their abundances at $t = 10^4$ yr. The results related to oxygen chemistry can be interpreted based on the detailed analysis by Charnley (1997). Water is the main parent molecule among oxygen-bearing species and mainly destroyed by HCO^+ to produce H_3O^+ in this model. This process keeps the HCO^+ abundance low where H_2O is injected from the grain mantles and is consistent with the result of Doty et al. (2002). Hydroxyl molecules are formed by the dissociative recombination of H_3O^+, so that the OH abundance changes discontinuously at the H_2O injection radius, $r_{\rm inj,H_2O}$. One of the destruction processes of carbon monoxide is the reaction with He^+, which makes atomic oxygen as well as atomic carbon. On the other hand, O and OH react with molecular hydrogen to reproduce water as $O \xrightarrow{H_2} OH \xrightarrow{H_2} H_2O$ at high temperature. Thus, the abundances of O and OH are suppressed in the inner hot region. These behaviours are also consistent with the results of Doty et al. (2002). The reaction between OH and N generates NO, which makes the radial abundance profile of NO similar to that of OH. Molecular oxygen is not only injected from the grain mantles but also synthesized from O and OH. HCO is principally produced by the destruction of H_2CO by OH, so that the

HCO abundance jump appears at $r_{\rm inj,H_2CO}$. C_3H_4 is chiefly formed initiated from C_2H_2 as $C_2H_2 \stackrel{HCO^+}{\longrightarrow} C_2H_3^+ \stackrel{CH_4}{\longrightarrow} C_3H_5^+ \stackrel{e}{\longrightarrow} C_3H_4$ in this model. Therefore, the C_3H_4 abundance increases over a radial distance between $r_{\rm inj,H_2O}$, inside which the HCO^+ abundance is suppressed, and $r_{\rm inj,C_2H_2}$.

Figures 2c and 4c are the time evolution of column densities and the radial abundance profiles of nitrogen-bearing species, whose detailed hot core chemistry have analysed by Millar et al. (1997) and Rodgers & Charnley (2001). The nitrogen molecule is the most dominant nitrogen-bearing species in the initial gas in this model, and is converted into N and N^+, through reaction with He^+. Ammonia is one of the possible nitrogen-bearing mantle species and is destroyed by ionized molecules to produce NH_2. Meanwhile, it is formed from gas-phase reactions initiated from N^+ as $N^+ \stackrel{H_2}{\longrightarrow} NH^+ \stackrel{H_2}{\longrightarrow} NH_2^+ \stackrel{H_2}{\longrightarrow} NH_3^+ \stackrel{H_2}{\longrightarrow} NH_4^+ \stackrel{e}{\longrightarrow} NH_3$. The radial abundance profile of HCN has two apparent discontinuous jumps in this model. One is at the radius where $\tau_{\rm acc,HCN} = \tau_{\rm evap,HCN}$ and the other is at $r_{\rm inj,H_2CO}$ as H_2CO is one of the main precursors of CH_2, which reacts with N to produce HCN. The major production reaction of HNC is that between NH_2 and C. Thus, the HNC abundance jumps at $r_{\rm inj,NH_3}$. CH_3CN is mainly produced by the radiative association between HCN and CH_3^+, so that the radial abundance profile of CH_3CN resembles that of HCN. The CH_3CN abundance is suppressed inside $r_{\rm inj,H_2O}$ because H_3^+, which helps produce CH_3^+ from its reaction with CH_3OH, decreases in abundance as it preferentially transfers its proton to the abundant water molecule. HC_3N is generated from N as $N \stackrel{C_3H}{\longrightarrow} C_3N \stackrel{XH^+}{\longrightarrow} HC_3N^+ \stackrel{H_2}{\longrightarrow} H_2C_3N^+ \stackrel{e}{\longrightarrow} HC_3N$. C_3H is a product of C_2H_2, which causes the HC_3N abundance jump at $r_{\rm inj,C_2H_2}$. CN is also chiefly formed from $H_2C_3N^+$ inside $r_{\rm inj,C_2H_2}$, but the jump does not appear in the CN abundance because CN can be synthesized by neutral-neutral reactions such as C+NO outside $r_{\rm inj,C_2H_2}$. The CN abundance is suppressed in the inner hot region due to the loss by a reaction with H_2 which creates HCN.

Figures 2d and 4d represent the time evolution of column densities and the radial abundance profiles of sulfur-bearing species, respectively. Their basic behaviour can be explained following the analyses by Millar et al. (1997) and Charnley (1997). Hydrogen sulfide is a possible sulfur-bearing grain mantle species, and can be easily destroyed by atomic hydrogen especially in the inner hot region because of the small activation energy barrier of this reaction. This drives the sulfur chemistry in hot cores as $H_2S \stackrel{H}{\longrightarrow} SH \stackrel{H}{\longrightarrow} S \stackrel{O_2}{\longrightarrow} SO \stackrel{OH}{\longrightarrow} SO_2$. Thus, the SO abundance is lowered inside $r_{\rm inj,H_2O}$, where the OH abundance is high, while the SO_2 abundance drops outside $r_{\rm inj,H_2O}$. Also, both the SO and SO_2 abundances change dramatically at $r_{\rm inj,O_2}$. NS is produced by the reaction between SH and N, so that the NS abundance changes discontinuously at $r_{\rm inj,H_2S}$. CS is mainly generated as $SO \stackrel{C}{\longrightarrow} CS$ in the inner region, while $HCS^+ \stackrel{e}{\longrightarrow} CS$ in the outer region. On the other hand, HCS^+ is synthesized by the proton transfer process to CS in the inner region, whereas by the reaction between CS^+ and H_2 in the outer region. Therefore, the radial abundance profiles of HCS^+ and CS resemble each other. OCS is injected from grain mantles in this model in order to represent the observed high abundance of OCS molecular lines, and based on the observations of ice absorption features by Palumbo et al. (1997) (see also discussions in Hatchell et al. 1998b).

Table 3. Initial abundances of mantle molecules for Model B.

Species	Abundance	Species	Abundance	Species	Abundance
C_2H_2	5.0×10^{-7}	CO_2	3.0×10^{-6}	O_2	1.0×10^{-6}
CH_4	2.0×10^{-7}	H_2CO	2.0×10^{-6}	H_2O	2.8×10^{-4}
C_2H_4	1.0×10^{-8}	CH_3OH	4.0×10^{-7}	NH_3	8.0×10^{-7}
C_2H_6	1.0×10^{-8}	C_2H_5OH	1.0×10^{-8}	H_2S	3.0×10^{-7}
				OCS	1.0×10^{-7}

Figures 2e and 4e show the time evolution of column densities and the radial abundance profiles of large oxygen-bearing species, which can be interpreted according to the analyses by Millar et al. (1991) and Charnley et al. (1992). Methanol is one of the possible large oxygen-bearing grain mantle molecules and is protonated by H_3^+. The product of the protonation, $CH_3OH_2^+$, leads to the formation of daughter molecules as $CH_3OH_2^+ \stackrel{H_2CO}{\longrightarrow} HCOOCH_4^+ \stackrel{e}{\longrightarrow} HCOOCH_3$ and $CH_3OH_2^+ \stackrel{CH_3OH}{\longrightarrow} C_2H_6OH^+ \stackrel{e}{\longrightarrow} (CH_3)_2O$. Thus, abundance jumps of $HCOOCH_3$ and $(CH_3)_2O$ appear at $r_{\rm inj,CH_3OH}$. CH_3CHO is mainly made by the reaction between atomic oxygen and C_2H_5 which is generated from C_2H_6, so that the CH_3CHO abundance changes dramatically at $r_{\rm inj,C_2H_6}$. CH_2CO is chiefly formed from the reactions of $C_2H_3 \stackrel{O}{\longrightarrow} CH_2CO$ and $CH_3^+ \stackrel{CO}{\longrightarrow} CH_3CO^+ \stackrel{e}{\longrightarrow} CH_2CO$ inside $r_{\rm inj,C_2H_4}$, while from the latter reaction otherwise. In this model C_2H_5OH is assumed to be created on dust grains in order to reproduce the observations of C_2H_5OH molecular lines (cf. Millar et al. 1997; Rodgers & Charnley 2001; Ikeda et al. 2001).

5. Discussion

5.1. Trapping of mantle molecules in water ice

It is known that water is one of the most abundant ice component in dense clouds. Some observations of ice absorption features in infrared spectra towards young stellar objects have suggested that a certain amount of CO is frozen in H_2O-rich matrices (e.g., review by Allamandola et al. 1999), and laboratory experiments have shown that solid CO is able to diffuse into the porous structure of H_2O and be trapped in it (Collings et al. 2003). These studies suggest that mantle molecules other than CO also could be trapped in water ice. Thus, in this subsection we examine the effects of this trapping on the chemical structure of the hot core G34.3+0.15. In order to see the extreme case, we put the injection radius of each mantle molecule as $r_{{\rm inj},i} \equiv r_{\rm inj,H_2O}$, and assume that it is completely trapped in H_2O matrices outside $r_{\rm inj,H_2O}$, except CO, for which we assume that $x({\rm CO}) = 0.3x({\rm H_2O})$ is trapped outside $r_{\rm inj,H_2O}$ based on

Table 4. Molecular column densities of Model B and observations.

	$N_{\rm mol}$ [cm^{-2}]			$N_{\rm mol}$ [cm^{-2}]	
Species	Model B[a]	Obs.	Species	Model B[a]	Obs.
CO	2.0×10^{20}	$>2.9\times10^{19}$	H_2S	2.4×10^{16}	$>1.1\times10^{16}$
C_2H	3.2×10^{15}	$>8.2\times10^{15}$	SO	9.7×10^{15}	$>2.4\times10^{15}$
CH_3C_2H	1.3×10^{12}	1.8×10^{16}	SO_2	2.3×10^{16}	9.3×10^{15}
H_2O	3.5×10^{19}	1.3×10^{19}	CS	1.5×10^{15}	1.0×10^{16}
H_2CO	2.3×10^{17}	$>2.3\times10^{16}$	OCS	1.9×10^{16}	$>1.8\times10^{16}$
HCO^+	5.5×10^{14}	$>1.4\times10^{15}$	H_2CS	1.8×10^{14}	$>3.8\times10^{16}$
HCO	6.4×10^{13}	$>5.3\times10^{13}$	HCS^+	5.6×10^{12}	$>3.0\times10^{13}$
NO	1.6×10^{16}	$>5.8\times10^{15}$	NS	5.0×10^{13}	$>4.0\times10^{13}$
NH_3[b]	2.6×10^{18}	$>2.7\times10^{18}$	CH_3OH	7.4×10^{16}	2.6×10^{16}
HNC	1.3×10^{15}	$<3.3\times10^{14}$	C_2H_5OH	1.8×10^{15}	1.7×10^{15}
HCN	5.0×10^{15}	1.2×10^{15}	CH_2CO	1.3×10^{14}	6.7×10^{14}
CN	1.3×10^{15}	$>5.9\times10^{14}$	CH_3CHO	1.3×10^{14}	2.4×10^{14}
HC_3N	1.1×10^{15}	$>2.5\times10^{13}$	$HCOOCH_3$	1.0×10^{15}	1.4×10^{15}
CH_3CN	3.4×10^{12}	$>2.4\times10^{14}$	CH_3OCH_3	5.5×10^{13}	3.7×10^{15}

[a] Calculated results at 10^4 yr.
[b] In the case of $\Theta_{\rm beam} = 0.025$ pc.

observations (e.g., Chiar et al. 1998; cf. Doty et al. 2002). As a result of the time-dependent chemical calculation described in Sect. 3, we get the molecular column densities of the hot core consistent with most of the observations at around 10^4 yr (Table 4). The initial condition listed in Table 3 is used in this calculation, which is slightly different from that in Table 1, in order to fit the results to the observations. Although there are few differences in the integrated molecular column densities, we find that very different structure appear in the radial profiles of molecular abundances at around 10^4 yr between the results in Sect. 4 (Fig. 4: Model A) and those obtained from this calculation (Fig. 5: Model B). Especially the differences are remarkable in the following molecules: (1) the binding energies of the molecules or their parent species are low, that is, the injection radii listed in Table 1 are large, such as H_2CO, HCO, H_2S, and SO, or (2) daughter molecules whose production are suppressed where H_2O is evaporated from grain mantle, such as CH_3C_2H and CH_3CN. For comparison, the resulting radial abundance profiles of SO and CH_3CN from Model A (dotted lines) and B (solid lines) are plotted in the linear radial scales in Fig. 6. Detailed observations of radial profiles of molecular abundances may make it possible to examine what fraction of molecules is trapped in water ice in cooler region of hot cores.

5.2. Dependence of chemical structure on density profile – General model

The comparison between the results of chemical calculation and the observations of various kinds of molecular lines will be useful to constrain the physical condition of massive star forming regions (e.g., Viti & Williams 1999). The density profile of hot molecular cores is one of the possible tracers of the evolution process just before and after massive star formation. In this section we will investigate the dependences of the chemical structure of hot cores on the density profile to discuss the physical condition of massive-star-forming clumps.

The chemical structures of three different types of molecular clumps are investigated here. Their density profiles are set by Eq. (1) with core radii of $r_{\rm c} = 0.01$, 0.05, and 0.1 pc, and plotted in Fig. 7a with dotted, solid, and dashed lines, respectively. Making use of these density profiles, we calculate the temperature profiles by solving the radiative transfer equation as described in Sect. 2.2. The resulting temperature distributions are shown in Fig. 7b. We can see from the figure that the temperature profiles directly reflect the difference in the density profiles. This is because the temperature profiles of hot cores are determined by the balance between the absorption of radiation from the central star and the reemission of the radiation by dust grains in the core as described by Eq. (2). The inner regions of the cores are optically thick enough to the radiation from the central stars so that the photons from the stars diffuse via interactions with the surrounding dusty material. If we simply assume that the dust opacity depends on the frequency of radiation as $\kappa_\nu \propto \nu^n$ and the density profile of a clump is set as $\rho \propto r^{-p}$, for example, the temperature profile of the clump illuminated by a central star is derived as $T \propto r^{-(p+1)/(4-n)}$ in the optically thick limit from the equation of local radiative equilibrium and the radiative transfer equation (e.g.,

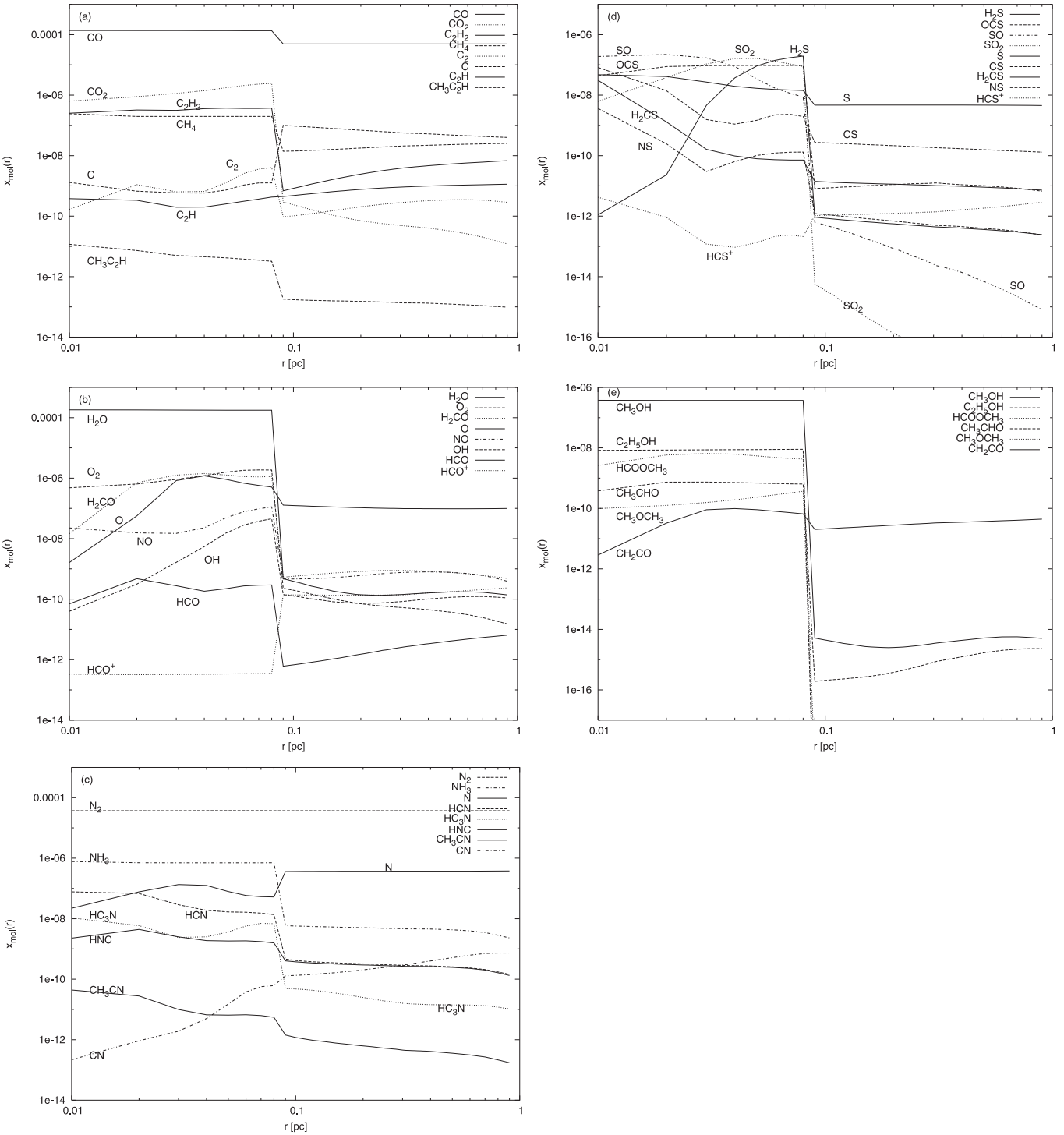

Fig. 5. The same as Fig. 4 but with the trapping of mantle molecules in water ice. Large differences appear in the radial distributions of some molecules compared to those in Fig. 4.

Adams & Shu 1985). Meanwhile, since the evaporation process of grain mantle species is very sensitive to the temperature as shown in Sect. 3, it is to be expected that the density profiles affect the radial abundance profiles of molecules in hot cores via the temperature profiles. In order to see the dependence on the density models clearly, the temperature profiles in the region of grain mantle evaporation are plotted with linear scales in Fig. 7c.

The luminosity of the central star is another factor that influences the temperature profile of the clump. As we can see from Figs. 7b, c, the temperature distribution of the clump whose core radius is $r_c = 0.05$ pc and whose central star luminosity is $L_* = 10^3\ L_\odot$ (dot-dashed lines) is similar to that of the model with $r_c = 0.01$ pc and $L_* = 10^5\ L_\odot$. The difference in luminosity will be, however, distinguishable by observing the spectral energy distribution. The hydrogen column density will

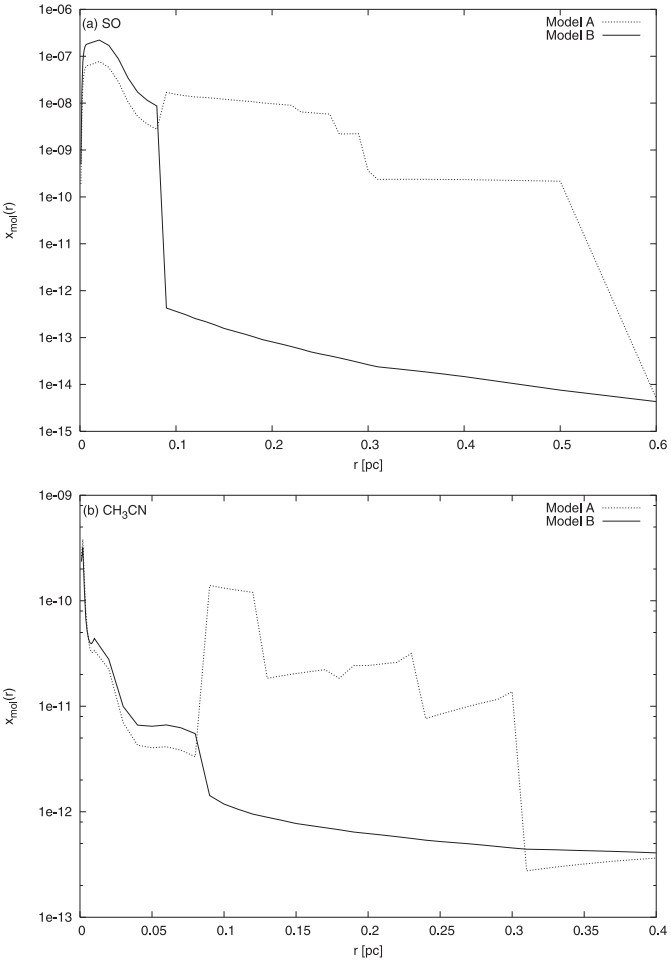

Fig. 6. The comparison of the radial abundance profiles of **a)** SO and **b)** CH_3CN in the linear radial scales between the models without (dotted lines: Model A) and with (solid lines: Model B) the trapping of mantle molecules in water ice. We can find the difference in the location of jump in **a)** and that the abundance is low through the clump in Model B in **b)**.

not have very much effect on the temperature structure in the optically thick region because basically $T(r)$ depends not on the absolute density but on the steepness of the density profile as we have shown in the above example. The optically thick region spreads (shrinks) if the hydrogen column density is high (low) so that it will affect the temperature profile at the outer radii.

We calculate the gas-phase chemical reactions in the clumps with the above density and temperature profiles and $L_* = 10^5\ L_\odot$ by means of the chemical model in Sect. 3. Figure 8 gives the resulting radial abundance profiles of some molecules at 10^4 yr in the linear radial scales (while those in Fig. 4 are scaled in the logarithmic manner). They are parent or daughter species and have dramatic changes at certain radii related to grain mantle evaporation. H_2O, CO_2, H_2CO, H_2S, C_2H_2, and CH_3OH are possible parent molecules, and have abundance jumps at their injection radii. The daughter species HC_3N, CH_3CN, and $HCOOCH_3$ are produced mainly from C_2H_2, HCN, and CH_3OH, respectively, in this model, and their abundance jumps appear at the same radii as those of the parent species. Comparison between reasonably high resolution observations of abundance jumps and precise radiative transfer and physical-chemical models of hot cores may make it possible to test the formation processes of these molecules.

From Fig. 8 we can see that the abundance jump of each molecule occurs at a smaller radius in the clump with a smaller core radius r_c, that is, with a steeper density and therefore a steeper temperature profile. The molecules in Fig. 8 can keep high fractional abundances only in the inner region of the clump (<0.1 pc) if $r_c = 0.01$ pc. This result suggests that the chemically rich hot cores, whose observational beam-averaged molecular column densities are large, have flat density profiles rather than steep ones. On the basis of the low and high mass star formation theories, the central density profiles of clumps are thought to be steep just after the star formation, at least if accretion of the surrounding material to the central protostellar cores is important (e.g., Shu 1977; Yorke & Bodenheimer 1999; Masunaga & Inutsuka 2000; Yorke & Sonnhalter 2002). Subsequently, dissipation by outflows will let the clumps gravitationally unbound and their central density profiles will be flattened (e.g., Shu et al. 1987; Nakano et al. 1995). In the case of massive star formation, powerful outflows with high mass loss rates as well as radiation pressure and strong winds from the stars may accelerate the dissipation process. If massive stars are formed as a result of coalescence of lower mass stars, the envelopes will have different density profiles from those of isolated star-forming clumps (e.g., Bonnell et al. 1998). Statistical observations of various kinds of molecular lines towards hot cores could constrain their density profiles and the massive star formation theories.

The effects of inflow motion of hot cores have not been considered in this paper. If the inflow has a velocity of a few km s^{-1} as is estimated from the observed atomic and molecular lines (e.g., Keto 2002), it will not affect the structure on the scale of about 0.25 pc, which corresponds to the observational beam size for most of the molecular lines we have used in this paper, within the timescale of 10^4 yr. Comparison between model calculations and the forthcoming high spatial resolution and high sensitivity observations could reveal the dependence of the chemical structure of hot cores on the inflow motion. In addition, the temporal evolution of young massive stars in hot cores is also a factor that may possibly influence the fractional abundances of some species (cf. Viti & Williams 1999).

6. Summary

We have constructed the density and temperature profiles of hot cores that have embedded luminous objects, using radiative transfer calculations together with observations of the spectral energy distribution. We have used these to investigate hot core chemistry taking into account the temperature dependent grain mantle evaporation process.

As a result of applying the model to the hot core G34.3+0.15 and calculating the time-dependent gas-phase reactions in hot gas heated by a central massive star, it is confirmed that the age of around 10^4 yr is preferred to reproduce the large column densities of both the parent and the

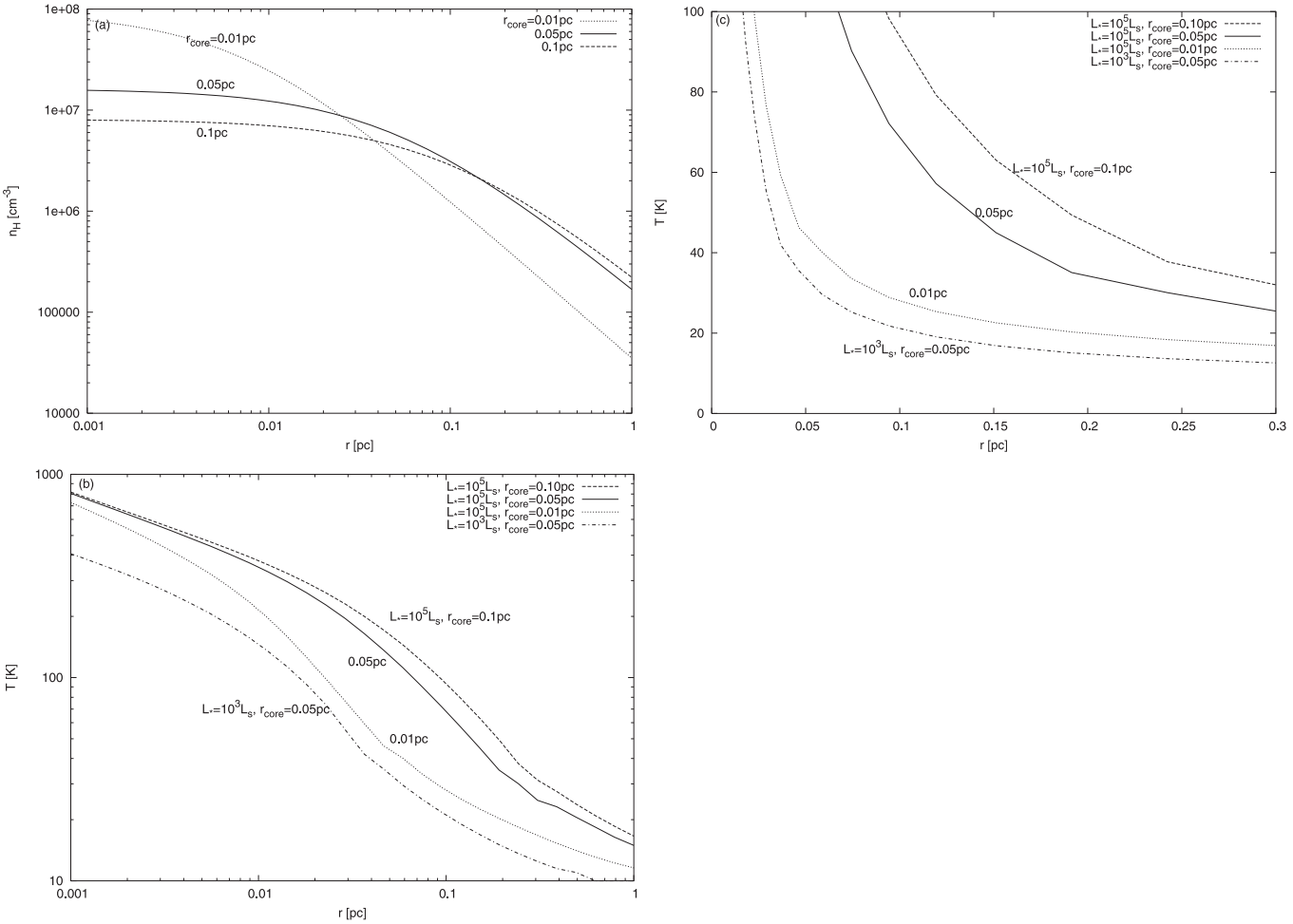

Fig. 7. a) Density and **b)** temperature profiles in the logarithmic scales for the models with $L_* = 10^5\ L_\odot$ and $r_c = 0.01$ (dotted lines), 0.05 (solid lines), and 0.1 pc (dashed lines). The temperature profiles directly reflect the difference in the density profiles. **c)** Temperature profiles in the linear scales represent clearly the dependence on the density models around the temperatures of grain mantle evaporation. Profiles of the model with $L_* = 10^3\ L_\odot$ and $r_c = 0.05$ pc (dot-dashed lines) are also plotted for comparison.

daughter molecules. In fact, the calculated column densities are consistent with most of those observed toward G34.3+0.15 around 10^4 years after central luminous star formation with a particular initial composition for the grain mantle molecules.

Also, we find that dramatic changes appear in the radial profiles of fractional abundances of some parent, daughter and related species at the parents' injection radii, inside which the evaporation time of the molecules from dust grains are shorter than their accretion time. The abundance jumps appear because (1) most of the parents are difficult to destroy within the timescale of 10^4 yr, and (2) the initial abundances of parents is large enough, so that despite their slow destruction rates inside the injection radii, they produce appreciable abundances of daughter products, while (3) these parent and daughter molecules are hardly produced by the gas-phase reactions outside the injection radii.

Finally, we discussed the influence of some chemical and physical properties on the chemical structure of hot cores. First, we investigated the effects of the trapping of mantle molecules in water ice. As a result, we find large changes in the location of jumps in the radial abundance profiles of some species and that it changes completely the radial abundance profiles of daughter molecules whose production are suppressed in regions where H_2O is evaporated from grain mantle. Also, we investigated the chemical structure of hot cores with different density profiles. Our results suggest that the chemically rich hot cores have flat density profiles rather than sharp ones. This is because a steeper radial density profile leads to a steeper temperature distribution as long as the clump is optically thick to radiation from the central star. This means that the abundance jumps appears at smaller radii and that therefore beam-averaged molecular column density cannot be large. Observational possibilities of constraining the density profiles of hot cores and the massive star formation theories are also suggested.

Acknowledgements. We would like to thank the referee, Dr. F.L. Schoier, for his comments which improved our paper. Astrophysics at UMIST is supported by a grant from PPARC.

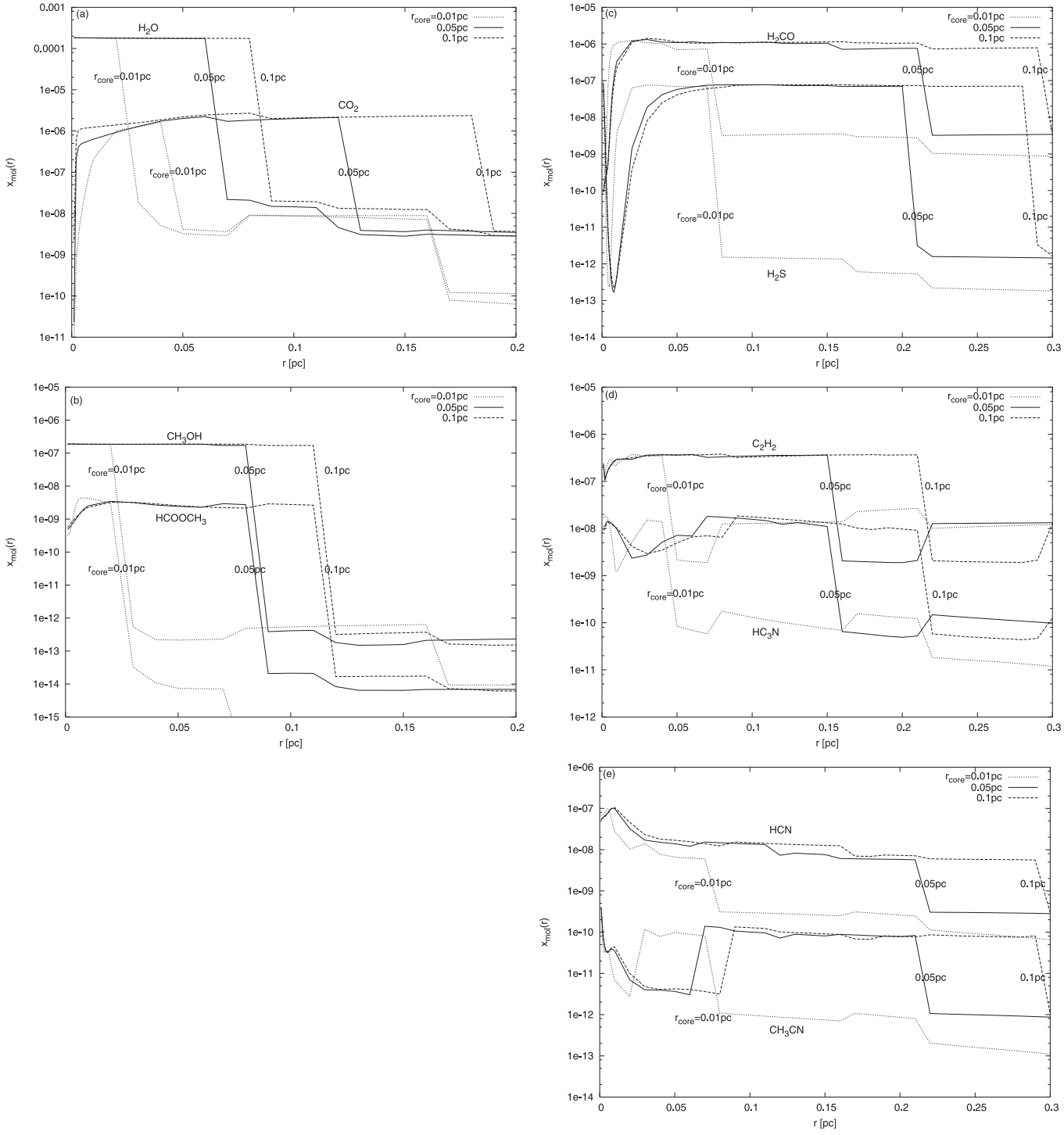

Fig. 8. The radial abundance profiles of some parent and daughter molecules of the models in the linear radial scales with $L_* = 10^5\ L_\odot$ and $r_c = 0.01$ (dotted lines), 0.05 (solid lines), and 0.1 pc (dashed lines). The abundance jumps appear at the inner radii in the models with the smaller core radii, that is, having steeper density and temperature profiles.

References

Adams, F. C., & Shu, F. H. 1985, ApJ, 296, 655

Adams, F. C., & Shu, F. H. 1986, ApJ, 308, 836

Aikawa, Y., Umebayashi, T., Nakano, T., & Miyama, S. M. 1997, ApJ, 486, L51

Allamandola, L. J., Bernstein, M. P., Sandford, S. A., & Walker, R. L. 1999, Space Sci. Rev., 90, 219

Bonnell, I. A., Bate, M. R., & Zinnecker, H. 1998, MNRAS, 298, 93

Bonner, W. B. 1956, MNRAS, 116, 351

Boonmann, A. M. S., van Dishoeck, E. F., Lahuis, F., Wright, C. M., & Doty, S. 2000, in ISO beyond the Peaks, ed. A. Salama, M. F. Kessler, K. Leech, & B. Schulz, ESA-SP 456, 67

Brown, P. D., Charnley, S. B., & Millar, T. J. 1988, MNRAS, 231, 409

Cardelli, J. A., Meyer, D. M., Jura, M., & Savage, B. D. 1996, ApJ, 467, 334

Caselli, P., & Myers, P. C. 1995, ApJ, 446, 665

Caselli, P., Hasegawa, T. I., & Herbst, E. 1993, ApJ, 408, 548

Charnley, S. B. 1997, ApJ, 481, 396
Charnley, S. B., Tielens, A. G. G. M., & Millar, T. J. 1992, ApJ, 399, L71
Chiar, J. E., Gerakines, P. A., Whittet, D. C. B., et al. 1998, ApJ, 498, 716
Chini, R., Krügel, E., & Wargau, W. 1987, A&A, 181, 378
Churchwell, E. 2002, ARA&A, 40, 27
Collings, M. P., Dever, J. W., Fraser, H. J., McCoustra, M. R. S., & Williams, D. A. 2003, ApJ, 583, 1058
Doty, S. D., & Neufeld, D. A. 1997, ApJ, 489, 122
Doty, S. D., van Dishoeck, E. F., van der Tak, F. F. S., & Boonman, A. M. S. 2002, A&A, 389, 446
Draine, B., & Lee, H. M. 1984, ApJ, 285, 89
Dullemond, C. P., & Turolla, R. 2000, A&A, 360, 1187
Ebert, R. 1955, Zs. Ap., 37, 217
Ehrenfreund, P., Dartois, E., Demyk, K., & D'Hendecourt, L. 1998, A&A, 339, L17
Falgarone, E., Puget, J.-L., & Pérault, M. 1992, A&A, 257, 715
Fraser, H. J., Collings, M. P., McCoustra, M. R. S., & Williams, D. A. 2001, MNRAS, 327, 1165
Fuller, G. A., & Myers, P. C. 1992, ApJ, 384, 523
Gerakines, P., Whittet, D. C. B., Ehrenfreund, P., et al. 1999, ApJ, 522, 357
Hasegawa, T. I., & Herbst, E. 1993, MNRAS, 261, 83
Hatchell, J., Fuller, G. A., Millar, T. J., Thompson, M. A., & Macdonald, G. H. 2000, A&A, 357, 637
Hatchell, J., Thompson, M. A., Millar, T. J., & Macdonald, G. H. 1998a, A&AS, 133, 29
Hatchell, J., Thompson, M. A., Millar, T. J., & Macdonald, G. H. 1998b, A&A, 338, 713
Heaton, B. D., Little, L. T., & Bishop, I. S. 1989, A&A, 213, 148
Henning, Th., Schreyer, K., Launhardt, R., & Burkert, A. 2000, A&A, 353, 211
Ikeda, M., Ohishi, M., Nummelin, A., et al. 2001, ApJ, 560, 792
Kaufman, M. J., Hollenbach, D. J., & Tielens, A. G. G. M. 1998, ApJ, 497, 276
Keane, J. V., Tielens, A. G. G. M., Boogert, A. C. A., Schutte, W. A., & Whittet, D. C. B. 2001, A&A, 376, 254
Keto, E. 2002, ApJ, 568, 754
Kim, H-D., Cho, S-H., Chang, H-S., et al. 2000, ApJS, 131, 483
Kurtz, S., Cesaroni, R., Churchwell, Ed., Hofner, P., & Walmsley, C. M. 2000, in Protostars and Planets IV, ed. V. G. Mannings, A. P. Boss, & S. S. Russell (Tuscon: Univ. Arizona Press), 299
Lahuis, F., & van Dishoeck, E. F. 2000, A&A, 355, 699
Larson, R. B. 1981, MNRAS, 194, 809
Larson, R. B. 1969, MNRAS, 145, 271
Macdonald, G. H., Gibb, A. G., Habing, R. J., & Millar, T. J. 1996, A&AS, 119, 333
Masunaga, H., & Inutsuka, S. 2000, ApJ, 531, 350
McLaughlin, D. E., & Pudritz, R. E. 1996, ApJ, 469, 194
Meyer, D. M., Cardelli, J. A., & Sofia, U. J. 1997, ApJ, 490, L103
Meyer, D. M., Jura, M., & Cardelli, J. A. 1998, ApJ, 493, 222
Millar, T. J. 1993, in Dust and Chemistry in Astronomy, ed. T. J. Millar, & D. A. Williams (Bristol: IOP Publishing), 249
Millar, T. J. 1997, in Molecules in Astrophysics: Probes and Processes, ed. E. F. van Dishoeck (Dordrecht: Kluwer), IAU Symp., 178, 75
Millar, T. J., Herbst, E., & Charnley, S. B. 1991, ApJ, 369, 147
Millar, T. J., Macdonald, G. H., & Gibb, A. G. 1997, A&A, 325, 1163
Millar, T. J., & Hatchell, J. 1998, Faraday Discussions, 109, 15
Myers, P. C., & Fuller, G. A. 1992, ApJ, 396, 631
Nakano, T., Hasegawa, T., & Norman, C. 1995, ApJ, 450, 183
Nomura, H. 2002, ApJ, 567, 587
Osorio, M., Lizano, S., & D'Alessio, P. 1999, 525, 808
Palumbo, M. E., Geballe, T. R., & Tielens, A. G. G. M. 1997, ApJ, 479, 839
Rawlings, J. M. C., Hartquist, T. W., Menten, K. M., & Williams, D. A. 1992, MNRAS, 255, 471
Rodgers, S. D., & Charnley, S. B. 2001, ApJ, 546, 324
Schöier, F. L., Jørgensen, J. K., van Dishoeck, E. F., & Balke, G. A. 2002, A&A, 390, 1001
Shu, F. H. 1977, ApJ, 214, 488
Shu, F. H., Adams, F. C., & Lizano, S. 1987, ARA&A, 25, 23
Stahler, S. W., Palla, F., & Ho, P. T. P. 2000, in Protostars and Planets IV, ed. V. G. Mannings, A. P. Boss, & S. S. Russell (Tuscon: Univ. Arizona Press), 327
Thompson, M. A., Macdonald, G. H., & Millar, T. J. 1999, A&A, 342, 809
Thompson, R. I. 1984, ApJ, 283, 165
Tielens, A. G. G. M., & Allamandola, L. J. 1987, in Interstellar Processes, ed. D. J. Hollenbach, & H. A. Thoronson Jr. (Dordrecht: Reidel), 397
Viti, S., & Williams, D. A. 1999, MNRAS, 305, 755
Watt, S., & Mundy, L. G. 1999, ApJS, 125, 143
Willacy, K. A., Klahr, H. H., Millar, T. J., & Henning, Th. 1998, A&A, 338, 995
Yorke, H. W., & Bodenheimer, P. 1999, ApJ, 525, 330
Yorke, H. W., & Sonnhalter, C. 2002, ApJ, 569, 846
van der Tak, F. F. S., van Dishoeck, E. F., Evans II, N. J., & Blake, G. A. 2000a, ApJ, 537, 283
van der Tak, F. F. S., van Dishoeck, E. F., & Caselli, P. 2000b, A&A, 361, 339